# Hyperbranched epoxy/modified clay nanocomposites

**Highlight**

This chapter deals with fabrication, characterization and property evaluation of hyperbranched epoxy and modified clay nanocomposites. The chapter is divided into two sub-chapters, where the first sub-chapter demonstrated tough and highly flexible nanocomposites of hyperbranched epoxy with first generation of poly(amido-amine) dendrimer modified bentonite nanoclay. The formation of partially exfoliated structure of the nanocomposites with good physico-chemical interactions among hyperbranched epoxy, poly(amido-amine) hardener and modified clay was investigated by FTIR, XRD, SEM, and TEM analyses. Significant improvements in performance of the pristine epoxy were achieved by the formation of nanocomposites with 3 wt% of modified clay. Thus, the studied epoxy nanocomposites have great potential to be used as an advanced epoxy thermoset. In the second sub-chapter, high performance, tough and antimicrobial hyperbranched epoxy nanocomposites were fabricated by the incorporation of neem-oil-immobilized organo-modified montmorillonite nanoclay. The dose-dependent enhancements of tensile strength, elongation at break, toughness and thermal stability of the pristine epoxy thermoset were observed for the nanocomposites along with significant antimicrobial activity against different bacteria and a fungus. Thus, these nanocomposites have strong potential as high performance antimicrobial materials.

---

Parts of this chapter are published in

1. B. De and N. Karak, *J. Appl. Polym. Sci*. **131**, 40327 (8 p), 2014.
2. B. De, K. Gupta, M. Mandal and N. Karak, *New J. Chem*. **39**, 595-603, 2015.

# 3A. Hyperbranched epoxy/poly(amido-amine) modified bentonite nanocomposites

## 3A.1. Introduction

In the first chapter, it is described that polymer nanotechnology is one of the most promising areas in this century to achieve extraordinary performance of polymers. The formation of polymer nanocomposites not only improves the existing properties of the virgin polymers but it also provides a new set of desired properties to expand the application area of them. Clay is one of the most widely used nanomaterials for the fabrication of polymer nanocomposites because of its layer structure with high aspect ratio, which allows efficient load tolerance of the matrix.[1-4] Thus, the formation of suitable epoxy/clay nanocomposites offers high mechanicals properties like tensile strength, modulus, flexural strength, hardness, etc. along with high thermal stability and other properties.[3-9] The basic principle for the improvement in performance of these clay nanocomposites is penetration and interaction of the polymer chains within the interlayer galleries of clay. In contrary, hydrophilic nature of the unmodified clay resulted high moisture absorption and incompatibility with the hydrophobic polymer matrix. Thus, different methods have been reported to make it hydrophobic for good dispersion in polymer matrices.[7-11] Among them alkylammonium cation exchange is a very common process to make hydrophobic clay for the preparation of polymer nanocomposites. However, it has been observed in most of the literature, such polymer/clay nanocomposites significantly improved only tensile strength, modulus, flexural strength and hardness. But, the desired flexibility, toughness and elongation at break are rare to achieve in all such cases.[12,13] In case of modified clay based epoxy nanocomposites, improvements in fracture toughness and modulus as well as in few cases tensile strength are also found in literature. Wang et al. reported epoxy nanocomposites with highly exfoliated clay where improvements of 80% stress intensity factor ($K_{IC}$), 190% critical strain energy release ($G_{IC}$) and 40% modulus were found with 2.5 wt% slurry clay.[4] The organoclay modified epoxy nanocomposites with improvements of 80% $K_{IC}$, 152% $G_{IC}$ and 20% modulus at 12 phr of organoclay was reported by Liu et al.[14] Zerda et al. reported intercalated clay/epoxy nanocomposites with 3.5 wt% clay for 100% improvement in $K_{IC}$ and $G_{IC}$.[15] A epoxy/clay nanocomposite with 50% enhancement in tensile strength, 77% improvement in $K_{IC}$ and 190% increment in $G_{IC}$ with 2 wt% clay was reported by Wang et al.[16] However, in all the above cases, a decrease in elongation at break and in few cases both elongation at break and tensile strength up to 50% was noticed and thus, a massive reduction in ductility is obvious. Balakrishnan et al. also

reported the increments of tensile modulus and strength, though ductility decreases with the increase of organoclay content in DGEBA based epoxy matrix.[17] Hence low ductility and toughness are common but serious drawbacks of epoxy thermoset, which remained unsolved.

Therefore, we reported a simple strategy to achieve the desired tensile strength, elongation at break, toughness and ductility of a hyperbranched epoxy nanocomposites by incorporation of hydrophobic aliphatic poly(amido-amine) dendrimer modified bentonite. In the present investigation the modified nanoclay may toughen and flexibilize the epoxy resin because of the unique structure of the modifying agent. Further, the amalgamation of this unique structural architecture of modifying agent with hyperbranched epoxy resin may provide strong physico-chemical interactions and thereby helping in improvement of overall performance of the resulted nanocomposites.

## 3A.2. Experimental

### *3A.2.1. Materials*

Triethanolamine (TEA) based hyperbranched epoxy resin was used in this study. The low cost, easy and liquid state availability as well as high boiling nature of TEA are the driving forces for this choice. Further, $A_2$ + $B_3$ is the most facile and popular approach for the synthesis of such hyperbranched polymers as described earlier also. Here TAHE20 resin was used as the matrix, as it possesses the overall best performance among other TAHE thermosets as mentioned in earlier chapter. Thus, the materials and processes were used in this study related to TAHE20 resin or thermoset are same as described in sub-chapter 2B.

In this study, hydrophilic bentonite clay was used for the fabrication of hyperbranched epoxy nanocomposites after modification. It was purchased from Sigma-Aldrich, Germany. The hydrophilic clay was modified with first generation of poly(amido-amine) dendrimer (PAD), obtained by the same procedure as reported in the sub-chapter 2B (used as a hardener) to render it organophilic nature.

### *3A.2.2. Characterization*

The characterization procedures and instrumentations for spectroscopic study, mechanical properties, adhesive strength, thermal properties, etc. were same as described in Chapter 2. Here, the morphology of the nanocomposites was studied by high resolution transmission electron microscope, HR-TEM (JEOL, JEMCXII, Transmission Electron Microscope operating voltage at 200 kV) and scanning electron microscope, SEM (JEOL, JSM-6390 LV). The crystalinity and the interlayer spacing of the clay were measured by X-ray

Diffractometer, Miniflex (Rigaku Corporation, Japan) using CuKα radiation (λ = 0.154 nm). Again, to account the interactions between modified clay and hyperbranched epoxy, the experimental modulus values of the nanocomposites were compared with the predicting values calculated from Guth generalized Einstein equation as well as Halpin-Tsai random and aligned parallel models. The experimental tensile modulus values of the nanocomposites were calculated from elastic region of the stress-strain profiles. The predicted modulus values were calculated from (1) Guth generalized Einstein's equation:[18,19]

$E_{NC} = E_M [1 + K_E V_f + 14.1(V_f)^2]$ …… (3A.1)

and (2) Halpin-Tsai (a) random model:[20-22]

$E_{NC} = E_M [(3/8)\{(1+\eta_L \xi V_f)/(1-\eta_L V_f)\} + (5/8)\{(1+2\eta_T V_f)/(1-\eta_T V_f)\}]$ …… (3A.2)

and (b) aligned parallel model:[20-22]

$E_{NC} = E_M [(1+\eta_L \xi V_f)/(1-\eta_L V_f)]$ …… (3A.3)

where $\eta_L = [(E_{NP}/E_M - 1)/(E_{NP}/E_M + \xi)]$ …… (3A.4)

and $\eta_T = [(E_{NP}/E_M - 1)/(E_{NP}/E_M + 2)]$ …… (3A.5)

Here, $E_{NC}$ and $E_M$ are the tensile modulus of the nanocomposites and the matrix respectively, $K_E$ is the Einstein's coefficient which is 0.67ξ (ξ is length to thickness ratio of clay) and $V_f$ is the volume fraction of the clay. The experimental modulus values were measured as slops of the linear portion (1-2% strain) of the stress-strain curves. The equation used for this purpose is y = mx + c, where m (modulus) is the slope, y is stress, x is strain and c is the constant.

### *3A.2.3. Methods*

3A.2.3.1. Modification of bentonite nanoclay by ammonium salt of PAD

For the modification of bentonite clay, at first the ammonium salt of PAD was prepared by the treatment of 2 g of PAD with 18 mL of aqueous HCl (1 N) at 70 °C for 2 h. The prepared ammonium salt was slowly added to the well dispersed aqueous clay (1 g) with constant stirring at room temperature. After complete addition of the salt, the temperature of the mixture was raised up to 70 °C and the conditions were maintained for another 4 h. Then the mixture was filtered and washed with water for several times for the complete removal of $Cl^-$ ions (checked by 0.1 M $AgNO_3$ solution). Finally, the treated clay was washed with THF for 2-3 times and then dispersed in THF (10 mg/mL). A little amount of this clay was dried under vacuum at 60 °C for the analysis.

3A.2.3.2. Preparation of TAHE20/modified clay nanocomposites

The hyperbranched epoxy/modified clay nanocomposites were prepared by *ex-situ* solution technique. The requisite amount (1, 3 and 5 wt%, separately) of the dispersed modified clay in THF was added into the hyperbranched epoxy and the mixture was stirred mechanically for 4 h followed by ultrasonication at 60% amplitude and 0.5 cycles (acoustic power density: 460 W/cm$^2$) for 10 min at 25-30 °C. Then, 50 wt% of PAA hardener was added to it and mixed homogeneously at room temperature. The mixture was coated on glass plates and steel plates for curing. Before curing, the plates were kept under vacuum at room temperature for 24 h to remove THF. Then, the plates were cured inside the furnace at 100 °C for specified time interval. The curing time was optimized by determining the swelling value. The cured nanocomposites were coded as MNC1, MNC3 and MNC5 for 1, 3 and 5 wt% modified clay, respectively. The nanocomposite of TAHE20 with 3 wt% of unmodified bentonite clay was also prepared for comparison purpose by using the same procedure and coded as BNC3.

## 3A.3. Results and discussion

### *3A.3.1. Modification and characterization of bentonite clay*

The hydrophilic bentonite clay was modified by alkyl ammonium ion exchange process. $Na^+$ ions of hydrophilic bentonite clay were exchanged by aliphatic poly(amido-ammonium) ions. The characteristic diffraction peak shifted from 2θ = 7.1° to 4.9° after modification (**Figure 3A.1a**). Thus basal spacing increases to 0.56 nm after modification as calculated from XRD data by Bragg's equation. This is due to the fact that the clay layers are intercalated by the branched structure of PAD modifying agent. In FTIR spectrum of modified clay (**Figure 3A.2**), the bands at 2932 cm$^{-1}$ indicated the presence of aliphatic –$CH_2$ stretching band. The others bands were observed at 3420, 1649, 1560, 1032, 524 and 452 cm$^{-1}$, which confirmed the presence of –NH and -OH, amide (C=O), interlayer $H_2O$, Si-O, Al-O-Si, Si-O-Si groups respectively.[5,6] But, in case of unmodified bentonite clay the band at 2932 cm$^{-1}$ was absent. The –OH stretching frequency of unmodified clay at 3446 cm$^{-1}$ was diminished as well as it became broad and appeared at 3420 cm$^{-1}$ for the modified clay. The interlayer $H_2O$ bending frequency of unmodified clay at 1641 cm$^{-1}$ was also diminished and shifted to 1565 cm$^{-1}$ for the modified clay. The hydrophobicity of the modified clay on incorporation of aliphatic PAD was also indirectly confirmed by TGA analysis, as no significant weight loss was observed near 100 °C. The thermograms of pristine and modified bentonite clay are shown in **Figure 3A.3a**. A continuous weight loss (11%) up to 100 °C of pristine bentonite was observed, which was almost insignificant (2%) for the modified system. This weight loss is due to the loss of structural and absorbed water molecules. Again, the unmodified hydrophilic

bentonite was thermally more stable and the weight residue found at 700 °C was 85%, while modified clay was continuously lost its weight and 78% weight residue was remained at 700 °C. This continuous and gradual loss of weight in the modified system is due to the degradation of aliphatic hydrocarbon of PAD.

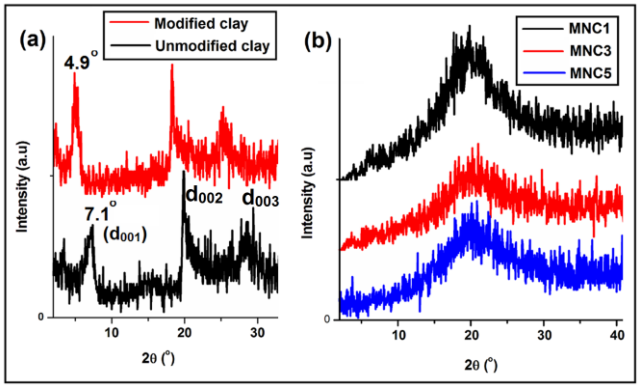


**Figure 3A.1:** XRD patterns of (a) pristine and modified bentonite, and (b) nanocomposites

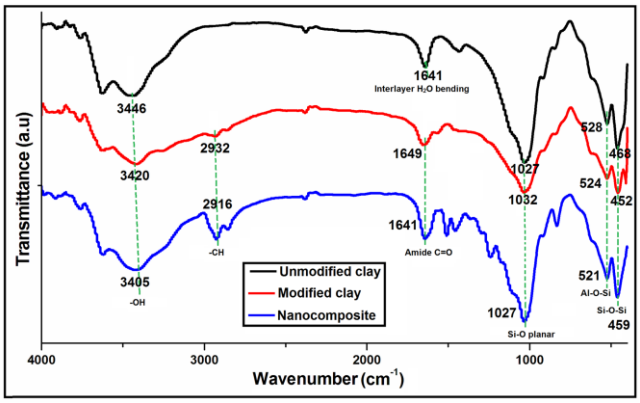


**Figure 3A.2:** FTIR spectra of pristine bentonite, modified bentonite and MNC3

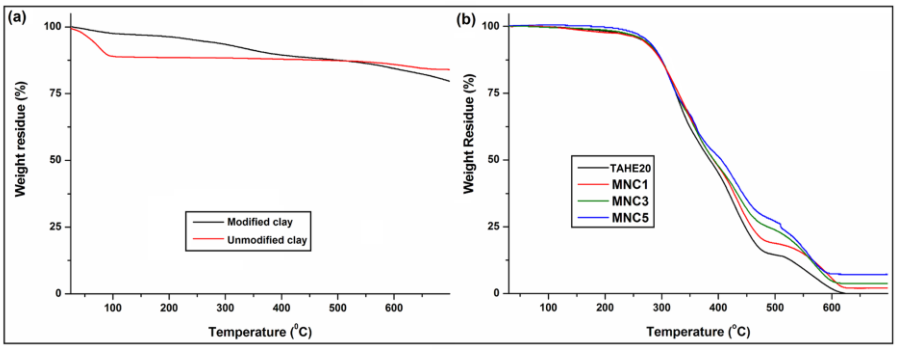


**Figure 3A.3:** (a) TGA thermograms of pristine and modified bentonite, and (b) pristine epoxy thermoset and nanocomposites

### *3A.3.2. Preparation and characterization of the nanocomposites*

The hyperbranched epoxy/modified clay nanocomposites were prepared by *ex-situ* solution technique using mechanical shearing force and ultrasonication. The curing time was optimized from the swelling value and the optimum cure time was taken at swelling value of 20-25% (80-75% gel fraction). The result of swelling values for TAHE20, MNC1, MNC3, and MNC5 was almost equivalent (24, 20, 21, and 22%). Thus the crosslink density is almost equal. The optimum curing time of the nanocomposites with 50 wt% PAA at 100 °C, decreases with the increases of clay content in the nanocomposites (**Table 3A.1**). This is due to the strong interactions of hyperbranched epoxy with the modified clay. The aliphatic PAD of the modified clay also took part in crosslinking reaction with the hyperbranched epoxy.

The diffraction peak for $d_{001}$ of the modified clay at $2\theta = 4.9°$ was completely diminished in nanocomposites as observed in XRD patterns (**Figure 3A.1b**). This may be due to the intercalation of polymer chain into the clay layers and also strong interactions like hydrogen bonding, polar-polar interactions, etc., which facilitate the well dispersions of clay layers with the epoxy. The presence of Si-O planar stretching and Al-O-Si, Si-O-Si bending of the clay in nanocomposites was confirmed by the FTIR bands at 1027 and 521, 459 $cm^{-1}$ respectively (**Figure 3A.2**).[5,6] The shifting of -OH band of modified clay in nanocomposites from 3420 to 3405 $cm^{-1}$ is due to the different physico-chemical interactions of clay with the hyperbranched epoxy. The TEM image discloses the actual picture of state of dispersion of clay in the nanocomposites. **Figure 3A.4a** clearly indicating the arrangement of clay layer in the matrix. Though the number of layers in a stack, but they are arranged in different directions and in some of the stacks, the number of layers is less. SEM is also a valuable technique for examining the morphology of the nanocomposites. SEM image of the fracture surface of the nanocomposite (**Figure 3A.4b**) also indicating the uniform dispersion of the clay layers as the surface morphology is quite rough for the studied matrix. This uniform dispersion is due to the strong physico-chemical interactions of aliphatic PAD of modified clay with hyperbranched epoxy and the hardener as shown in **Scheme 3A.1**.

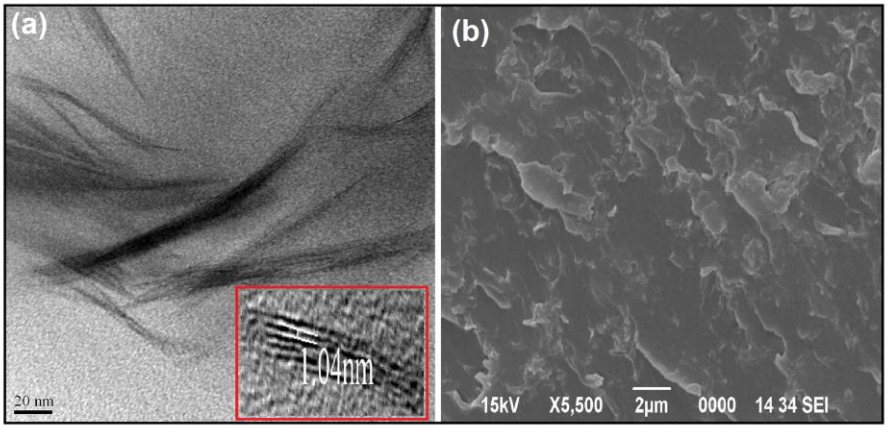


**Figure 3A.4:** (a) TEM and (b) SEM images of MNC3

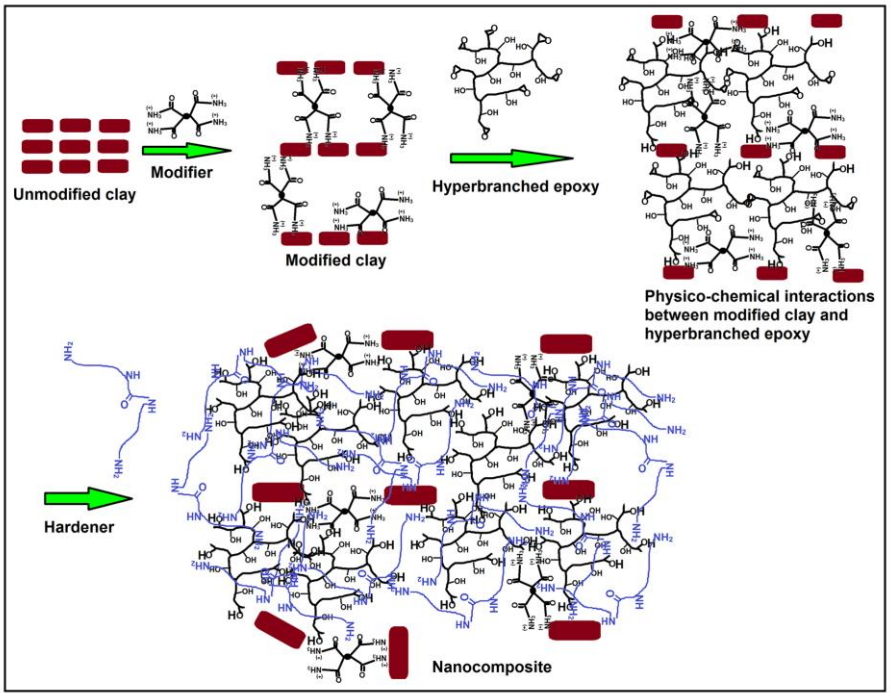


**Scheme 3A.1:** Different physico-chemical interactions of modified clay with hyperbranched epoxy and hardener based on the Halpin-Tsai aligned parallel model

**Table 3A.1:** Performance of the nanocomposites

| Parameter | TAHE20* | MNC1 | MNC3 | MNC5 | BNC3 |
|---|---|---|---|---|---|
| Curing time at 100 °C (min) | 75 | 70 | 55 | 45 | 90 |
| Swelling value (%) at 25 °C | 24±0.2 | 20±0.2 | 21±0.2 | 22±0.4 | 34±0.8 |
| Tensile strength (MPa) | 40±1 | 46±2 | 57±4 | 41±1 | 17.5±2 |
| Elongation at break (%) | 21±1 | 33.5±2 | 43±1.5 | 54±3 | 55±4 |
| Toughness (MPa) | 540±12 | 897±8 | 1804±14 | 1626±17 | 827±7 |
| Impact resistance (cm) | >100 | >100 | >100 | >100 | 95 |
| Scratch hardness (kg) | 9.0 | >10.0 | >10.0 | >10.0 | 8.5 |
| Bending dia. (mm) | <1 | <1 | <1 | <1 | <1 |
| Adhesive strength (W-W) (MPa) | 2680±30 | 4348±20 | 4393±40 | 4414±15 | 3422±40 |
| Adhesive strength (M-M) (MPa) | 2662±15 | 6698±18 | 6748±12 | 6740±16 | 3658±22 |

*As reported in sub-chapter 2A

### *3A.3.3. Mechanical properties of the nanocomposites*

The mechanical properties of the nanocomposites with different amount of clay loading are given in **Table 3A.1**. The interesting results in this study are the achievement of excellent toughness and high flexibility of the nanocomposites. The toughness of the nanocomposites as determined by integrating the stress-strain curves was sharply increased with the increase of amount of clay and thus, the nanocomposites behave like ductile materials. This is due to the combined effects of the flexible hydrocarbon chains of the aliphatic PAD, the modifying agent; different flexible moieties of hyperbranched epoxy and the long chain hydrocarbon part of the fatty acid of PAA hardener with the aromatic rigid moiety and clay platelets. The plasticizing effect of these flexible moieties has definite role for the above results. Again, both hyperbranched epoxy and PAD help to increase the free volume between the molecules because of their confined geometry, as reported in the previous chapter. It is also possible that clay platelets act both as physical and chemical crosslinkers (**Scheme 3A.1**). Both platelet motion and long range intercalations through physical crosslinks are potential candidates for the observed toughening of hyperbranched epoxy.[12] The elongation at break was also sharply increased with the increase of the amount of clay loading (**Figure 3A.5a**). It has been proposed that the increased elongation at break of polymer-clay nanocomposites may result

from the mobility of exfoliated clay platelets, which provides a mode for energy dissipation.[12] The tensile strength value of the hyperbranched epoxy thermoset was increased on incorporation of clay up to 3 wt% of loading, though the same was almost remained unchanged at 5 wt% loading. This is due to the agglomeration of clay particles in the polymer matrix at high loading. The impact strength and scratch hardness were also very high for the nanocomposites. The nanocomposites were exhibited high flexibility as they can be bent up to the lowest diameter of a mandrel (1 mm) or 180° without any damage or fracture for the same reason. As both the nanocomposites and the pristine epoxy were reached the highest limit of the instrument of the impact resistance (100 cm) and flexibility (1 mm), the enhancement of these values could not determine. The nanocomposites were also reached the highest limit of the instrument of the scratch hardness value (10.0 kg). However, due to the very poor interactions, the clay particles were separated out from the hyperbranched epoxy matrix and thus BNC3 exhibited low performance (**Table 3A.1**). This is due to the hydrophilic nature of the unmodified clay resulted high moisture absorption and less compatibility with the epoxy matrix and thus, they may agglomerate inside the matrix.

Again, mathematical modeling plays an important role in predicting properties of a polymer nanocomposite as well as to account the different interactions between nanomaterial and polymer matrix. The incorporation of rigid platelets of clay to the polymer matrices can produce number of effects like increment of strength, stiffness, modulus, fracture toughness, etc. These increments in properties of nanocomposites are affected by number of parameters such as shape, size, aspect ratio, volume fraction and distribution of the reinforcing nanomaterials. In literature, a number of theories and equations have been developed to describe these phenomenon.[18-22] But, here we have chosen those models which represented the best fitting of the experimental data. To account the polymer-filler interactions and for prediction of the modulus of the nanocomposites Guth generalized Einstein equation and Halpin-Tsai random and aligned parallel mechanical models were used (**Figure 3A.5b**). The experimental modulus values of the nanocomposites were matched with the Halpin-Tsai aligned parallel mechanical model (**Figure 3A.5b** and **Table 3A.2**) at low amount of clay content (1 and 3 wt%). However, at high amount of clay content (5 wt%) the experimental modulus value was deviated from this model. This is due to the aggregation of clay platelet in the matrix at high amount of clay content. But, at high amount of clay content (5 wt%), the experimental modulus value was matched with the Guth model (**Figure 3A.5b**). This is due to the fact that the Guth model considered only electrostatic and van der Waal's interactions (physical interactions) between the fillers and the matrix.[18] However, as in MNC1 and MNC3

both physical and chemical interactions are present their experimental modulus values are much higher compared to the values predicted by Guth model (**Table 3A.2**).

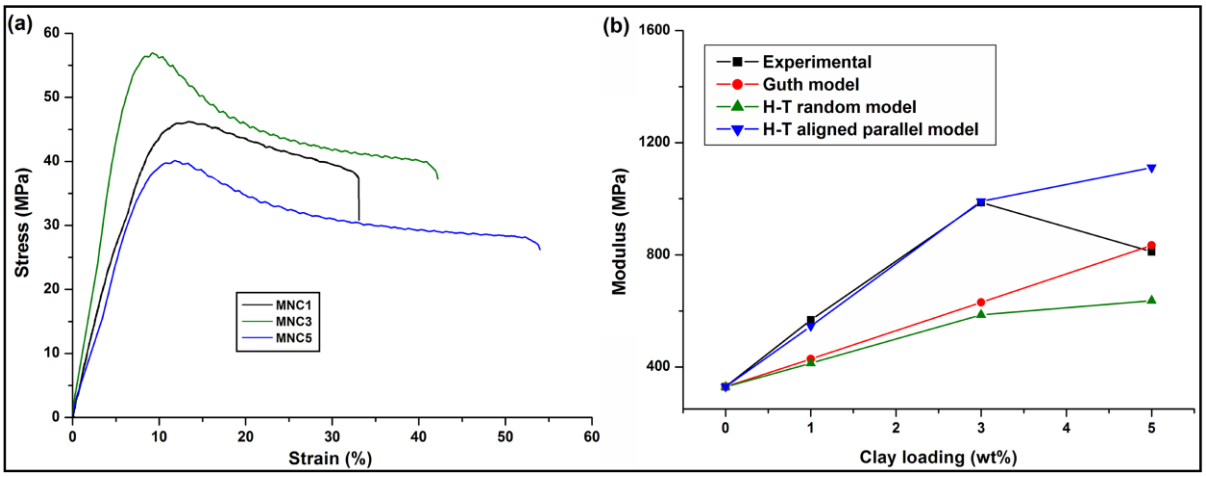


**Figure 3A.5:** (a) Stress-strain profiles of the nanocomposites and (b) plots of tensile modulus of predicted and experimental values of nanocomposites

**Table 3A.2:** Predicted and experimental modulus values (MPa)

| Mechanical model | TAHE20 | MNC1 | MNC3 | MNC5 |
|---|---|---|---|---|
| Guth generalized Einstein equation | 329 | 428 | 630 | 834 |
| Halpin-Tsai random model | 329 | 413 | 586 | 637 |
| Halpin-Tsai aligned parallel model | 329 | 546 | 991 | 1111 |
| Experimental value* | 329 | 568 | 987 | 807 |

*Calculated from stress-strain curves

### *3A.3.4. Adhesive strength of the nanocomposites*

Two fold improvement in adhesive strength both for wood-wood (W-W) and metal-metal (M-M) substrates was found after formation of nanocomposites (**Table 3A.1**). This is due to the presence of highly polar oxygen and nitrogen containing groups of epoxy, hardener and clay, which help to generate strong interaction with the cellulosic wood substrates. The branched architecture of hyperbranched epoxy, PAD and clay nanoparticles also help to physical interlocking with the metal substrates.[5] The diffusion of clay dispersed hyperbranched epoxy and hardener into the metal substrates helps to strong physical interlocking. Due to the same reasons slight improvement in adhesive strength was observed in BNC3. However, because of the poor interactions of unmodified hydrophilic clay with epoxy matrix the improvement is not significant.

### *3A.3.5. Thermal stability of the nanocomposites*

Slight increment in thermal stability and weight residue was observed for the thermoset as shown in TGA thermograms (**Figure 3A.3b**) after formation of nanocomposites. This is due to the presence of large numbers of aliphatic moieties of hyperbranched epoxy, hardener and aliphatic PAD. Different physico-chemical interactions of the matrix and the modifying agent with the clay platelets slightly improved the thermal stability. However, the weight residues of nanocomposites were increased due to the presence of clay platelets, which are thermostable even at 700 °C.

## 3A.4. Conclusion

An outstanding tough and flexible hyperbranched epoxy/aliphatic poly(amido-amine) modified bentonite nanocomposite with high elongation at break and adhesive strength was demonstrated. A significant improvement in toughness was observed from the area under the stress-strain curves. The simultaneous increment in tensile strength and elongation at break resulted in ductility of the nanocomposites and is a very exciting achievement, which was rarely found. Thus, this study may provide a new insight into the epoxy/clay nanocomposites for their future exploration. The unique characters like high strength, toughness and ductility render the nanocomposites as highly potential materials for engineering applications.

# 3B. Hyperbranched epoxy/neem-oil-modified OMMT nanocomposites

## 3B.1. Introduction

Incorporation of nanoclays into various polymers to enhance the properties like, mechanical, thermal, physical, barrier, etc. has been extensively reported over the last two decades.[1-9] High surface area, favorable intercalation chemistry and natural availability of clays make them most popular among all the nanomaterials.[3,4] The previous sub-chapter also demonstrates significant improvement in toughness along with other mechanical properties of hyperbranched epoxy thermoset by the incorporation of organically modified nanoclay. Again, nanoclays have high tendency to absorb or intercalate different bio-molecules like drugs or biocides,[5,23] organo-molecules[24] or different nanoparticles[25,26] between their layer structures and thus, recently they have attracted great attention in biological field. Therefore, biocide immobilized organophilic nanoclay will be an interesting proposition for the fabrication of hyperbranched epoxy/clay nanocomposites to enhance the application area by achieving high performance advanced antimicrobial material. Antimicrobial polymer nanocomposites are promising materials as binders for active surface coating for destructing or inhibiting the microorganisms in different fields including marine industries because of their slow releasing capability of the active agents. Traditionally antimicrobial materials contain one or more toxic compounds like biocides, metal nanopaticles, etc., which may cause human health as well as environmental hazards due to blooming and blushing problems.[27-29] In this regards, natural antibiotic or biopesticide immobilized clay reinforced polymer nanocomposite is preferred, though such report is rarely found.[5] The used active agent, *Homalomena aromatica* essential oil also faced problem of volatility and availability as reported in the literature.[5] On the other hand, among different natural biocides, neem (*Azadirachta indica*) seed oil is a very common and popular agent because of its non toxic nature to mammals as well as it is a very effective antiseptic, antifungal, antibacterial and insecticide.[30,31] Crude neem seed oil contains azadirachtin like biocidal triterpenoid compounds as well as long chain fatty acids like linoleic, oleic, palmitic, stearic, etc. acids.[32,33]

Thus, in this sub-chapter crude neem seed oil immobilized organically modified montmorilonite clay (OMMT) is used for the fabrication of high performance antimicrobial hyperbranched epoxy nanocomposite. Here, neem-oil will act as an antimicrobial agent as well as the fatty acids of the oil may toughen the whole system by plasticizing effect. In this

study, OMMT helps in enhancing the performance of the matrix as well as provides stability to the active agent.

## 3B.2. Experimental

### *3B.2.1. Materials*

Here also TAHE20 resin is used as the matrix for the preparation of nanocomposites like previous sub-chapter.

In this study, octadecyl amine modified montmorilonite nanoclay (OMMT) was used after immobilization of natural biocide. OMMT is the most widely used nanoclay for the preparation of polymer nanocomposites and it provides the best performance to the polymer matrices among all other nanoclays.[5,6,34-36] It was purchased from Sigma Aldrich, Germany.

Crude neem (*Azadirachta indica*) seed oil (NO) was used as the natural biocide for this study. It was immobilized on OMMT nanoclay. NO was acquired from Agri Life, India. It mainly contains azadirachtin like biocidal triterpenoid compounds as well as long chain fatty acids like linoleic acid, oleic acis, palmitic acid, stearic acid, etc. as shown in **Figure 3B.1**.

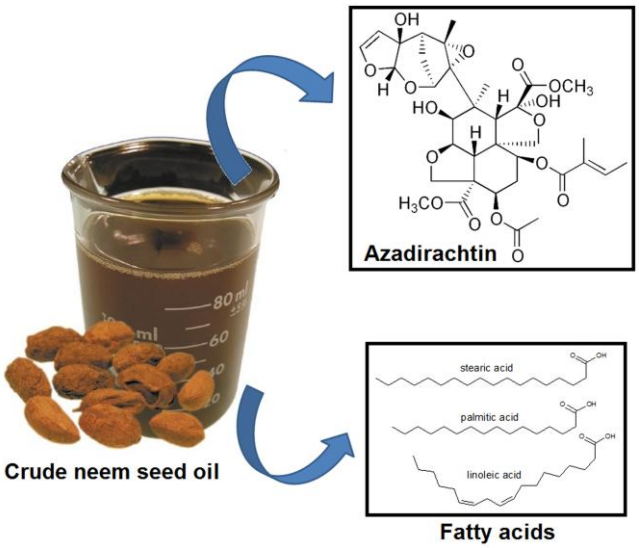


**Figure 3B.1:** Crude neem seed oil (NO) and its major compositions

All other materials like solvents, PAA hardener, etc. used in this sub-chapter were same as described in the previous sub-chapter.

### *3B.2.2. Characterization*

The instrumentation and characterization techniques including mechanical properties, thermal stability, chemical resistance, etc. tests were same as reported in the previous sub-chapter as well as in Chapter 2.

### *3B.2.3. Methods*

3B.2.3.1. Immobilization of NO on OMMT

NO was immobilized on OMMT by using mechanical and ultrasonic forces at room temperature. In a typical process, 0.5 g OMMT was dispersed in 25 mL THF by magnetic stirring for 30 min in a 60 mL glass bottle. An amount of 20 wt% of NO (0.1 g) was added into it and stirred continuously for 5 h and followed by ultrasonication for 10 min at room temperature. NO immobilized OMMT was coded as NO-OMMT. In order to study the effect of excess NO, OMMT was immobilized with 50 wt% of NO (with respect to OMMT) and coded as ENO-OMMT.

3B.2.3.2. Preparation of nanocomposites

The hyperbranched epoxy/NO-OMMT nanocomposites were prepared by solution technique as reported in the previous sub-chapter. Three different weight percentages (1, 2.5 and 5) of NO-OMMT dispersed in THF were incorporated into the hyperbranched epoxy, separately and stirred magnetically for 5 h at room temperature followed by ultrasonication for 10 min using same ultrasonic processor as described in previous sub-chapter. An amount of 50 wt% (with respect to hyperbranched epoxy) PAA hardener was mixed homogeneously with the above mixtures and coated on glass and steel plates. The plates were kept 24 h under vacuum at room temperature to remove THF and other volatiles. Initially (when the samples were in low viscous state) high vacuum was applied to remove THF and then the coated plates were kept on a flat platform to obtain even surface of the cast film. The samples were kept again under controlled vacuum. Two consecutive weights after 24 h and 30 h of the above coated plates were taken to confirm complete removal of THF or other volatiles. During this period only touch free of the samples was occurred, however no significant crosslinking was observed (swelling value 72%). Finally, the plates were cured inside a furnace at 100 °C for 60 min and followed by post-curing at 130 °C for 30 min. The nanocomposites were coded as PNC1, PNC2.5 and PNC5 for 1, 2.5 and 5 wt% NO modified OMMT respectively. Similarly, hyperbranched epoxy nanocomposite with 2.5 wt% unmodified OMMT was prepared (coded as PC2.5) for the comparison purpose. In order to study the effect of excess NO, a 2.5 wt% ENO-OMMT based nanocomposite was prepared and coded as PENC2.5.

3B.2.3.3. Antimicrobial study of the nanocomposites

Antimicrobial tests were done by well diffusion method as reported in the first chapter as well as in literature.[37,38] *Staphylococcus aureus* (MTCC 3160) and *Bacillus subtilis* (MTCC 121) as gram positive; *Klebsiella pneumoniae* (MTCC 618) and *Pseudomonas diminuta* (MTCC 3361) as gram negative bacterial stains and *Candida albicans* (MTCC 3017) as a fungus were used for antimicrobial assay. An amount of 200 μL of a log phase culture of the test microbes was seeded on the surface of the Muller Hinton agar (potato dextrose agar for fungal study) on petridishes. The nanocomposites were dispersed in sterilized DMSO and 100 μL of them put into the wells of diameter 6 mm. In one well DMSO was taken as blank and in another well Gentamicin (Nystatin for fungal) was used as a positive control. The zone of inhibition diameters were measured using a transparent ruler after incubated for 24 h at 37 °C (for bacteria) and for 48 h at 28 °C (for fungus). For growth curves analysis of the microbes, the cultures were taken in conical flasks. 200 μL of the samples were added to the corresponding conical flasks and incubated for 24 h at 37 °C (for bacteria) and for 48 h at 28 °C (for fungus). One conical flask without sample was taken as the control for the test of each microbe. The growth of the microbes was measured by checking optical density (OD) or absorbance at 620 nm after every 2 h and the OD was taken up to 20 h.

3B.2.3.4. Biofilm formation study

Biofilm formation on TAHE20 and PENC2.5 was studied by means of microtiter plate biofilm assay.[6,39] In the present study slight modification was done, here direct thermoset films (size 1 $cm^2$) were used instead of microtiter plates. The films were incubated for 72 h in potato dextrose broth (PDB) medium. The films were gently washed thrice with phosphate buffer saline (PBS, pH 7.4) to remove the planktonic bacteria. Then the films were resuspended and homogenized in PBS by rigorous vortexing for 5 min and the cells were serially diluted and plated onto PDB agar. Finally, colony-forming units (CFU) were enumerated after 48 h of incubation at 28 °C.

## 3B.3. Results and discussion

### *3B.3.1. Formation and characterization of NO-OMMT*

NO-OMMT was formed by the combined effect of mechanical shearing and ultrasonication forces. These forces help in dispersion of OMMT and interaction of its layers by NO due to the presence of polar groups in both. Immobilization of NO into OMMT was first characterized by FTIR study (**Figure 3B.2**). In FTIR spectra, the following bands were

found. For NO, $\nu_{max}$ ($cm^{-1}$): 3472 (-OH), 2928 (-CH), 1750 (C=O, ester) and 1458 (C-O, ester); and for OMMT, $\nu_{max}$ ($cm^{-1}$): 3640 (-NH), 3414 (-OH), 2928 (-CH), 1037 (Si-O), 527 (Al-O-Si) and 462 (Si-O-Si).[5,26] Whereas, the bands were observed in case of NO-OMMT, $\nu_{max}/cm^{-1}$: 3627 (-NH), 3427 (-OH), 2928 (-CH), 1736 (C=O, ester), 1627 (C=O, amide), 1471 (C-O, ester), 1037 (Si-O), 527 (Al-O-Si) and 462 (Si-O-Si). The shifting of ester linkages (C=O and C-O) of NO from 1750 and 1458 $cm^{-1}$ to 1736 and 1471 $cm^{-1}$ in NO-OMMT, reveals the presence of different interactions like hydrogen bonding, different polar-polar interactions, etc. of the NO with the OMMT clay. The presence of amide linkage in NO-OMMT along with ester linkage confirms that few ester groups of NO chemically interact with the amine groups (octadecyl amine) of OMMT. Interaction of NO with the clay galleries was also confirmed by XRD study (**Figure 3B.3**). In the XRD patterns, the basal peak ($d_{001}$) of OMMT was shifted from $2\theta = 4.2°$ to 2.7° after immobilization of NO. Thus, layer spacing increased by 1.17 nm after immobilization as calculated from XRD data from Bragg's equation. This shifting confirmed that NO is immobilized into the clay galleries and the fatty ester chains of NO intercalated into the layers by interacting with them.

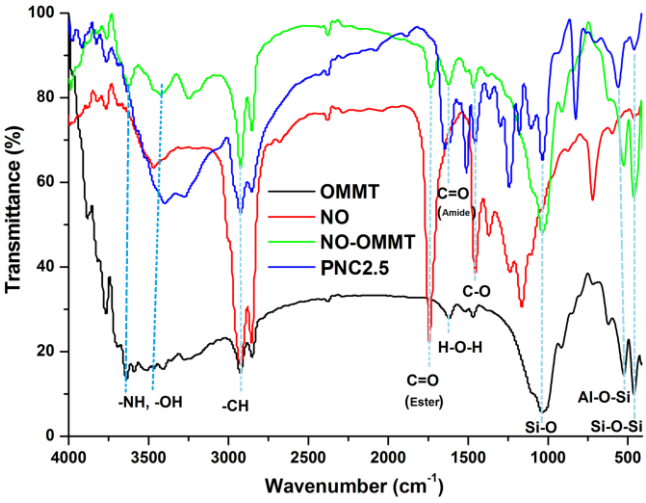


**Figure 3B.2:** FTIR spectra of OMMT, NO, NO-OMMT and nanocomposite (PNC2.5)

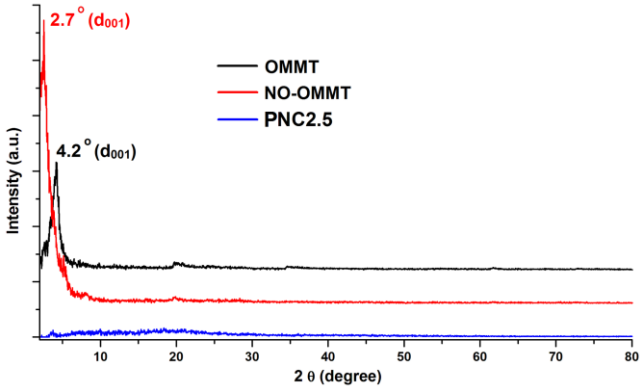


**Figure 3B.3:** XRD patterns of OMMT, NO-OMMT and PNC2.5

### *3B.3.2. Formation and characterization of the nanocomposites*

The hyperbranched epoxy/NO-OMMT nanocomposites were prepared by *ex-situ* solution technique by the combined effect of mechanical shearing force and ultrasonication. Compositions of the components in nanocomposites are given in **Table 3B.1**. The prepared nanocomposites were characterized by FTIR, XRD, SEM and TEM analyses. In FTIR spectrum of PNC2.5 (**Figure 3B.2**), the bands were found at $\nu_{max}$ ($cm^{-1}$): 3400 (-OH), 2928 (-CH), 1640 (C=O, amide), 1458 (C-O), 1037 (Si-O), 565 (Al-O-Si) and 462 (Si-O-Si).[5,6,26] Here shiftings of –OH and Al-O-Si bands of NO-OMMT from 3427 to 3400 and from 527 to 565 $cm^{-1}$ after formation of nanocomposite are due to the presence of different interactions like hydrogen bonding, different polar-polar, etc. interactions of NO-OMMT with the hyperbranched epoxy and PAA hardener. In the nanocomposite the ester linkage of NO-OMMT at 1736 $cm^{-1}$ was completely vanished, where only amide linkage was found at 1640 $cm^{-1}$. This confirmed that all the ester linkages of NO-OMMT are completely chemically reacted with the hardener during the curing time and converted into amide linkages. In the XRD pattern, $d_{001}$ diffraction peak of NO-OMMT at $2\theta = 2.7°$ was completely vanished after formation of nanocomposite (PNC2.5) as shown in **Figure 3B.3**. This may be due to the strong interactions of the polymer chains with clay galleries which cause complete delamination of the clay layers. It may also happens due to the masking effect of the clay with the polymer as the amount of clay was very low (2.5 wt%). The TEM images (**Figure 3B.4**) disclose the actual picture of the structure of the nanocomposites. The images reveal the intercalated structure of the NO-OMMT layers in hyperbranched epoxy matrix. This intercalated structure is due to the strong physico-chemical interactions of the chains of hyperbranched epoxy with NO-OMMT galleries which result uniform dispersion of the platelets in the matrix. The intercalated interlayer spacing of nanocomposite is shown in

**Figure 3B.4b**. The strong dispersion of NO-OMMT clay in the hyperbranched epoxy matrix was found from the SEM image of the fracture surface of the nanocomposite. From the SEM images, it can be seen that the surface of the nanocomposite, PNC2.5 (**Figure 3B.5b**) is rougher than the pristine hyperbranched epoxy, TAHE20 (**Figure 3B.5a**). This implies that the crack propagation will be less in rougher surface from the planner manner, as the crack tip is distorted by clay platelets and thus, crack propagation will be more difficult.[40]

**Table 3B.1:** Composition of nanocomposites in weight (phr)

| Component | PC2.5 | PNC1 | PNC2.5 | PNC5 | PENC2.5 |
|---|---|---|---|---|---|
| TAHE20 | 100 | 100 | 100 | 100 | 100 |
| PAA | 50 | 50 | 50 | 50 | 50 |
| OMMT | 2.5 | 0.83 | 2.08 | 4.17 | 1.67 |
| NO | 0 | 0.17 | 0.42 | 0.83 | 0.83 |

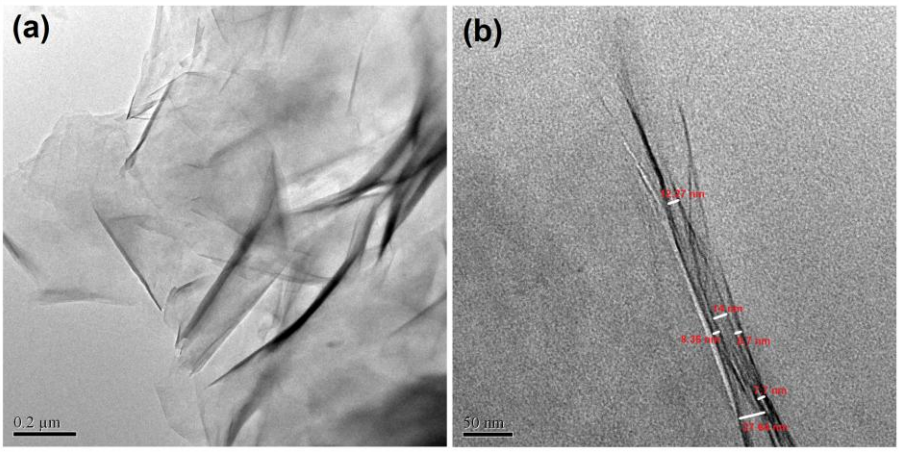


**Figure 3B.4:** TEM images of PNC2.5, (a) 200 nm and (b) 50 nm magnification

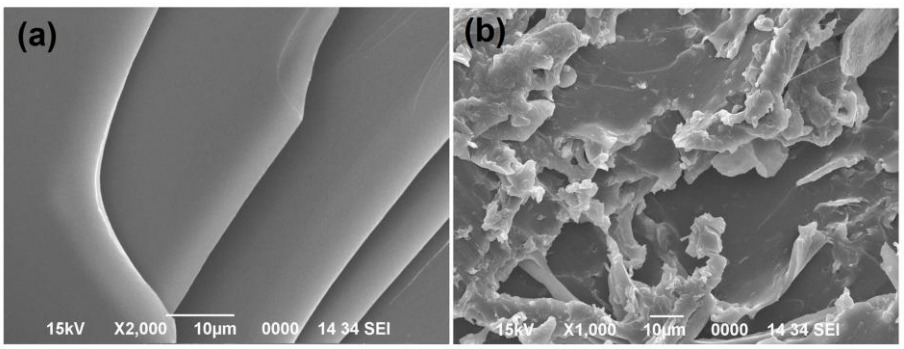


**Figure 3B.5:** SEM images of the fracture surface of (a) pristine hyperbranched epoxy thermoset (TAHE20) and (b) nanocomposite (PNC2.5)

### *3B.3.3. Curing study*

Curing study of the nanocomposites was done with 50 wt% of PAA hardener at 100 °C for 1 h and followed by post curing at 130 °C for 30 min. Swelling value of the thermosets was checked in THF at room temperature (25 °C). From **Table 3B.2** it is found that the swelling value of TAHE20 decreased after formation of nanocomposites both with unmodified OMMT (PC2.5) and NO-OMMT at lower amount (PNC1). However, the swelling values of the nanocomposites increased at higher amount of NO-OMMT (PNC5) and immobilized higher amount of NO (PENC2.5). This may be due to the fact that at higher amount of NO-OMMT or immobilized excess NO, the fatty ester of NO provides plasticizing effect, which in turn results and thus, large free volume to the system. This may help to penetrate the solvent molecules easily into the system.

### *3B.3.4. Mechanical properties of the nanocomposites*

Mechanical properties of the pristine hyperbranched epoxy thermoset and its nanocomposites with unmodified and NO modified OMMT are given in **Table 3B.2**. Here, more than 50% increment of tensile strength and more than 3 fold increment of elongation at break were found for hyperbranched epoxy thermoset after formation of nanocomposite with 2.5 wt% of NO-OMMT. However, 40% increment of tensile strength and no change in elongation at break were observed after formation of nanocomposite with 2.5 wt% of unmodified OMMT. Thus, the increment of toughness i.e. the area under stress-strain curves (**Figure 3B.6**) of hyperbranched epoxy thermoset was much higher in PNC2.5 (2994 MPa) than PC2.5 (834 MPa). This is because of plasticizing effect of fatty ester chains of NO inside the clay platelets which increases flexibility and toughness of the material by increasing free volume among the molecules through embedding them into hyperbranched epoxy chains and spacing them apart.[41] Thus, it provides more means of energy dissipation by the segmental motion of the aliphatic ester moieties in their molecular chains.[42,43] The energy dissipation is also possible through the mobility of clay platelets due to the sliding of the clay layers assisted through NO.[44] It has already been shown through the XRD study that NO increased the spacing (1.17 nm) between the clay layers which helps to penetrate the hyperbranched epoxy chains into the clay galleries. This helps in formation of strong interactions between polymer chains and clay layers, in turn of which the tensile strength enhances significantly. Elongation at break increases with the increase of amount of NO-OMMT or immobilized higher amount of NO (in case of PENC2.5). This is due to increase of plasticization effect of NO. However, tensile strength is decreased at higher loading of NO-OMMT (PNC5) and high amount of

immobilized NO (PENC2.5). This is because of decrease in interactions between hyperbranched epoxy and clay platelets at higher amount of clay loading may due to aggregation. Whereas, in case of high amount of immobilized NO the amount of aliphatic fatty ester chains are increased in the whole system, which provides more plasticizing effect to the system. The nanocomposites were exhibited high scratch hardness, impact resistance and flexibility as the toughness of the hyperbranched epoxy was increased dramatically after formation of nanocomposites. However, these differences could not be measured as the values for the nanocomposites reached the highest limit of the instruments for scratch hardness (10 kg), impact resistance (100 cm) and flexibility evaluation (1 mm bending diameter of mandrel). Nanocomposites absorbed the highest limit of impact energy, this is due to the presence of aliphatic fatty esters of NO and ether linkages of hyperbranched epoxy which dissipate the impact energy by the segmental motion of their molecular chains.[41,42]

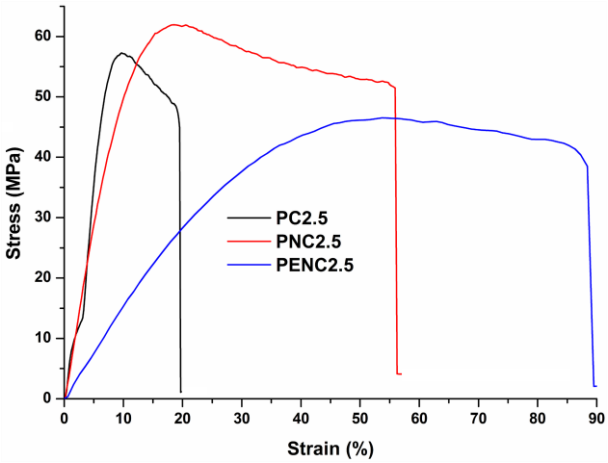


**Figure 3B.6:** Stress-strain profiles of the nanocomposites

**Table 3B.2:** Performance of pristine hyperbranched epoxy and its nanocomposites

| Parameter | TAHE20* | PC2.5 | PNC1 | PNC2.5 | PNC5 | PENC2.5 |
|---|---|---|---|---|---|---|
| Swelling value (%) | 24±0.2 | 21±0.4 | 22±0.8 | 24±0.2 | 29±0.6 | 34±1.1 |
| Tensile strength (MPa) | 40±1 | 57±1 | 48±4 | 62±3 | 56±2 | 46.5±2 |
| Elongation at break (%) | 21±1 | 19±1.5 | 43±2 | 56±5 | 69±4 | 88±4 |
| Toughness (MPa) | 540±12 | 834 | 1637 | 2994 | 2680 | 3323 |
| Scratch hardness (kg) | 9.0 | 10.0 | >10.0 | >10.0 | >10.0 | 10 |
| Impact resistance (cm) | >100 | >100 | >100 | >100 | >100 | >100 |
| Bending diameter (mm) | <1 | <1 | <1 | <1 | <1 | <1 |
| Initial degradation temperature (°C) | 267 | 282 | 278 | 285 | 288 | 279 |

*As reported in sub-chapter 2A

### *3B.3.5. Antimicrobial activity of the nanocomposites*

NO has been used as a biopesticide for long time.[30,31] The antibacterial activity of PNC1, PNC2.5 and PNC5 is shown in **Figure 3B.7**. From the figure, it can be seen that the nanocomposite exhibited significant antimicrobial activity towards gram positive as well as gram negative bacterial strain. The bacterial zones of inhibition for the nanocomposites were found in the range of 16-18 mm as shown in **Figure 3B.8a**. However, from **Figure 3B.8b**, it can be seen that PNC1, PNC2.5 and PNC5 cannot show significant antifungal activity. A little antifungal activity was observed after incorporation of 10 wt% NO-OMMT to the system (**Figure 3B.8b**). Whereas, PENC2.5 exhibited significant antifungal activity towards *C. albicans* fungal strain as shown in **Figure 3B.8c**. The fungal growth curves for the nanocomposites PNC1, PNC2.5, PNC5 and PENC2.5 are shown in **Figure 3B.8d**. Where, it can be seen that nanocomposites inhibit more fungal growth compared to the control. The antifungal activity increases with the increase of amount of NO-OMMT and immobilized higher amount of NO (PENC2.5). The bacterial growth curves for PNC1, PNC2.5, PNC5 and PENC2.5 are shown in **Figure 3B.9** with gram positive (*B. subtilis* and *S. aureus*) as well as gram negative (*K. pneumoniae* and *P. aeruginosa*) bacterial strains. In the figure, the bacterial growth decreases with the increase of amount of NO-OMMT and immobilized higher amount of NO (PENC2.5). From this study, it was found that PENC2.5 exhibited the highest antimicrobial activity.

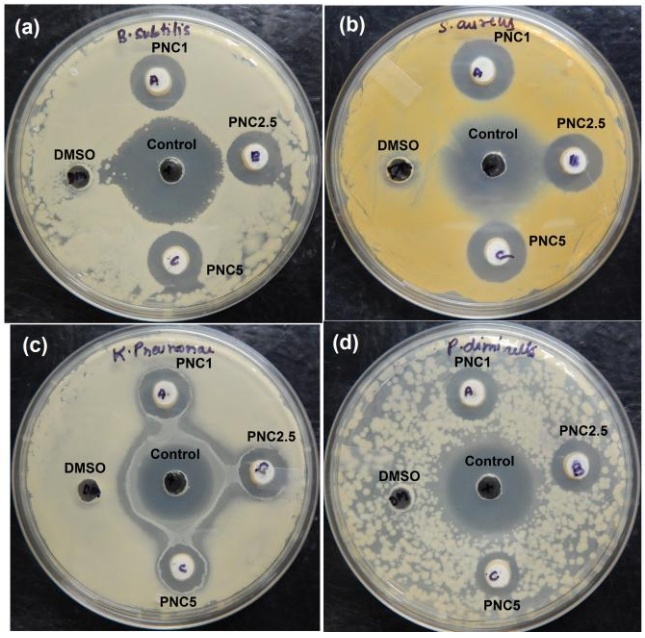


**Figure 3B.7:** Antibacterial activity of the nanocomposites

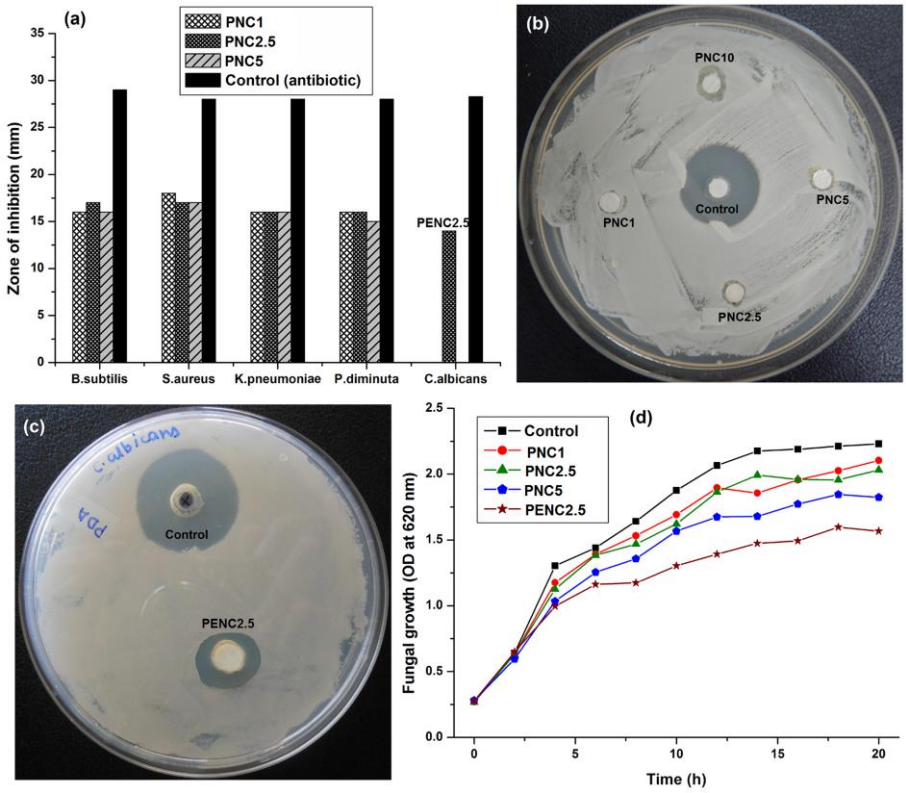


**Figure 3B.8:** (a) Zones of inhibition of the nanocomposites against different bacteria and *C. albicans* fungus (b) antifungal activity of the nanocomposites (c) antifungal activity of PENC2.5 and (d) fungal growth curves of the nanocomposites

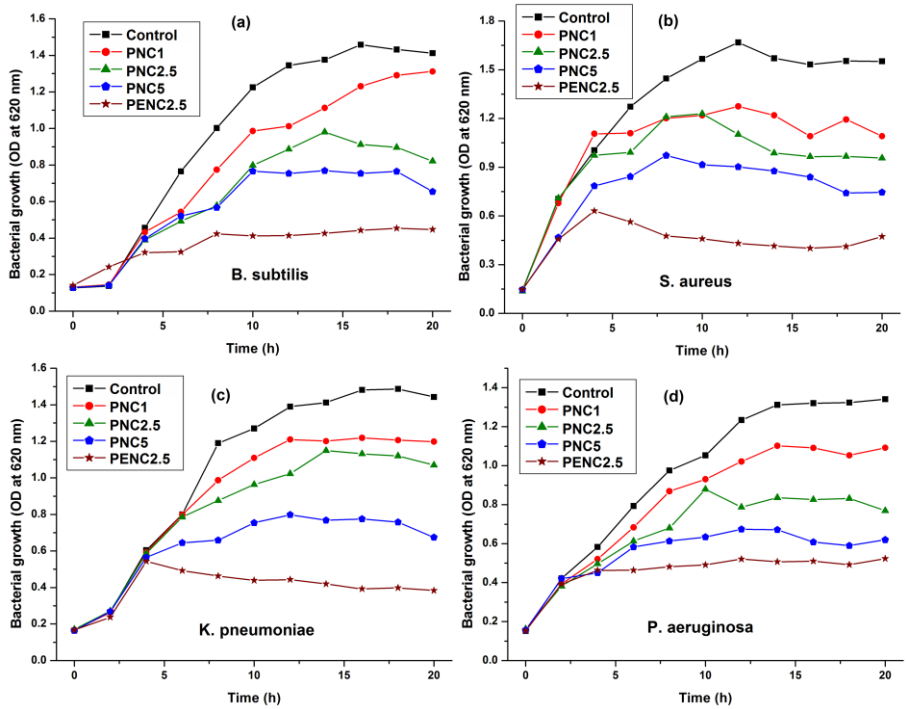


**Figure 3B.9:** Bacterial growth curves for the nanocomposites

### *3B.3.6. Biofilm formation study*

Biofilm formation study was done only for TAHE20 and PENC2.5 against *C. albicans* fungal strain. **Figure 3B.10** showed adherence of more number of fungus on TAHE20 film compared to PENC2.5. Thus, it is clearly visible that PENC2.5 inhibited more fungal adherence from the surface compared to TAHE20 and this is due to the presence of NO on OMMT surface of the nanocomposite. The presence of aliphatic fatty ester chains of NO in the system also increases the hydrophobicity of the thermoset, which inhibits the fungal adherence on the surface.

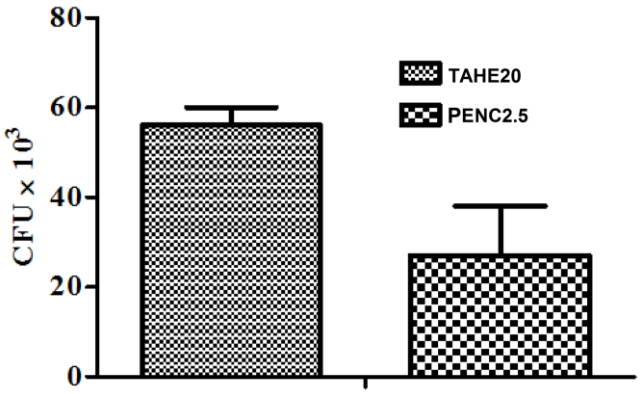


**Figure 3B.10:** Number of *C. albicans* adherence on the surface of TAHE20 and PENC2.5

### *3B.3.7. Thermal stability of the nanocomposites*

Thermal stability of the pristine hyperbranched epoxy was increased up to 15-20 °C after formation of nanocomposites with NO-OMMT as shown in **Figure 3B.11**. The initial (5% weight loss) thermal degradation temperature of the pristine hyperbranched epoxy thermoset and its nanocomposites are given in **Table 3B.2**. The thermal stability of the nanocomposites increases with the increase of amount of NO-OMMT, however it decreases with the increase of amount of immobilized NO. When the amount of NO increases the amount of aliphatic fatty ester also increased in the system, which is thermally less stable and thus overall thermal stability decreases. However, this thermal stability is much higher than the pristine thermoset. The reason for increase of thermal stability of pristine thermoset after formation of nanocomposites is due to the intercalation of clay galleries with hyperbranched epoxy and poly(amido-amine) chains, which restricted the segmental motion of the polymer chains by different physico-chemical interactions.[45] In addition to the above, the improvement in thermostability of the nanocomposite by incorporation of OMMT is due to the fact that clay is a heat insulator and acts as a mass transport barrier to the volatile products generated

during decomposition by providing longer paths for them to travel.[6] However, the amount of weight residue at 700 °C is found to be haphazard (**Figure 3B.11**) may be due to volatilization of the modified nanomaterial, which contains thermolabile aliphatic chains.

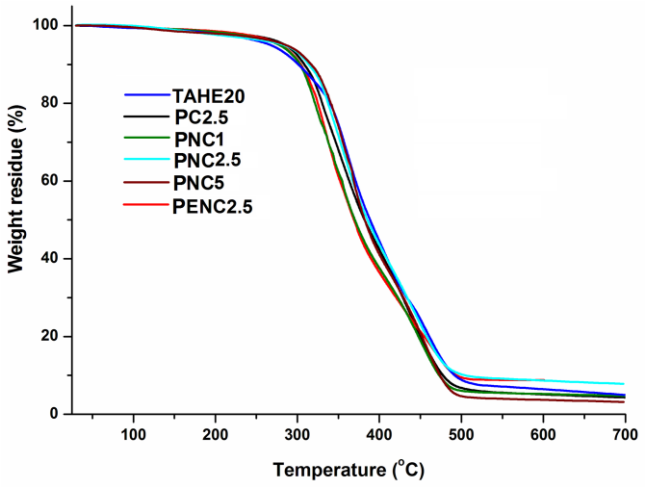


**Figure 3B.11:** TGA thermograms of pristine thermoset and the nanocomposites

### *3B.3.8. Chemical resistance of the nanocomposites*

The chemical resistance of pristine thermoset and its nanocomposites was tested in 5% aq. NaOH, 10% aq. HCl, 20% aq. NaCl, 20% aq. EtOH and tap water for 30 days of exposure and the percentage of weight loss of the samples was measured as given in **Table 3B.3**. The chemical resistance mainly depends on the crosslink density and number of chemically stable linkages present in the system. In case of polymer nanocomposites, it also depends on the interactions between polymer and nanomaterial. A little amount of weight loss was observed both in pristine hyperbranched epoxy thermoset as well as in nanocomposite films. The percentage of weight loss of nanocomposites at different chemical environments was increased at high amount of NO-OMMT (PNC5) and immobilized higher amount of NO (PENC2.5). This may be due to the plasticizing effect of fatty ester of NO. This creates large free volume to the system which may help to penetrate the chemicals. These penetrated chemicals degrade the uncured parts of the thermosets and thus, weight loss was observed. PNC1, PNC2.5 and PC2.5 showed superior chemical resistance to the pristine system due to the presence of stronger physico-chemical interactions like polar-polar, hydrogen bonding, intermolecular, mutual crosslinking, etc., between the matrix and the clay layers by strong dispersion of clay platelets into the matrix.[6]

**Table 3B.3:** Percentage of weight loss in different chemical media after 30 days of exposure

| Chemical medium | TAHE20* | PC2.5 | PNC1 | PNC2.5 | PNC5 | PENC2.5 |
|---|---|---|---|---|---|---|
| Aq. NaOH (5%) | 1.48 | 1.24 | 1.43 | 1.52 | 1.69 | 2.32 |
| Aq. HCl (10%) | 0.90 | 0.87 | 0.82 | 0.90 | 1.02 | 1.92 |
| Aq. NaCl (20%) | 0. 24 | 0.22 | 0.24 | 0.33 | 0.45 | 0.97 |
| Aq. EtOH (20%) | 0 | 0 | 0 | 0 | 0 | 0 |
| Water | 0 | 0 | 0 | 0 | 0 | 0 |

*As reported in sub-chapter 2A

### 3B.4. Conclusion

The present study demonstrated a facile approach to obtain thermosetting nanocomposite with significant antimicrobial activity, high mechanical performance, good thermal stability and high chemical resistance through the incorporation of neem seed oil immobilized organo modified montmorilonite in hyperbranched epoxy matrix. The investigation also paves a way to address the main drawbacks of brittleness and low toughness characters of epoxy thermoset. The intrinsic nature of neem seed oil as a biopesticide provides antimicrobial activity against different bacterial (both gram positive and gram negative) and fungal strains. Thus, the study opens up a new avenue for polymer nanocomposite to achieve antimicrobial functional material by incorporating neem-oil modified nanomaterial for its potential industrial application.

### References

1. Chen, B., et al. A critical appraisal of polymer-clay nanocomposites, *Chem. Soc. Rev*. **37**, 568--594, 2008.
2. Bragancüa, F. C., et al. Counterion effect on the morphological and mechanical properties of polymer-clay nanocomposites prepared in an aqueous medium, *Chem. Mater.* **19**, 3334--3342, 2007.
3. Park, J. H. & Jana, S. C. Mechanism of exfoliation of nanoclay particles in epoxy-clay nanocomposites, *Macromolecules* **36**, 2758--2768, 2003.
4. Wang, K., et al. Epoxy nanocomposites with highly exfoliated clay: mechanical properties and fracture mechanisms, *Macromolecules* **38**, 788--800, 2005.
5. Barua, S., et al. Biocompatible high performance hyperbranched epoxy/clay nanocomposite as an implantable material, *Biomed. Mater*. **9**, 025006 (14pp), 2014.

6. Roy, B., et al. Modified hyperbranched epoxy/clay nanocomposites: A study on thermal, antimicrobial and biodegradation properties, *Int. J. Mater. Res*. **105**, 296--307, 2014.
7. Jagtap, S. B., et al. Preparation of flexible epoxy/clay nanocomposites: effect of preparation method, clay modifier and matrix ductility, *J. Reinf. Plast. Compos*. **32**, 183--196, 2013.
8. Wang, W.S., et al. Properties of novel epoxy/clay nanocomposites prepared with a reactive phosphorus-containing organoclay, *Polymer* **49**, 4826--4836, 2008.
9. Kornmanna, X., et al. Synthesis of epoxy-clay nanocomposites: influence of the nature of the clay on structure, *Polymer* **42**, 1303--1310, 2001.
10. Lopez, G., et al. Influence of clay modification process in PA6-layered silicate nanocomposite properties, *Polymer* **46**, 2758--2765, 2005.
11. Khoeini, M., et al. Investigation of the modification process and morphology of organosilane modified nanoclay, *Ceram. Silikaty* **53**, 254--259, 2009.
12. Wang, J., et al. Significant and concurrent enhancement of stiffness, strength, and toughness for paraffin wax through organoclay addition, *Adv. Mater.* **18**, 1585--1588, 2006.
13. Shah, D., et al. Dramatic enhancement in toughness of polyvinylidene fluoride nanocomposites via nanocly-directed crystal structure and morphology, *Adv. Mater.* **16**, 1173--1177, 2004.
14. Liu, W., et al. Organoclay-modified high performance epoxy nanocomposites, *Compos. Sci. Technol*. **65**, 307--316, 2005.
15. Zerda, A. S. & Lesser, A. J. Intercalated clay nanocomposites: morphology, mechanics, and fracture behavior, *J. Polym. Sci., Part B: Polym. Phys*. **39**, 1137--1146, 2001.
16. Wang, L., et al. Preparation, morphology and thermal/mechanical properties of epoxy/nanoclay composite, *Composites Part A* **37**, 1890--1896, 2006.
17. Balakrishnan, S., et al. The influence of clay and elastomer concentration on the morphology and fracture energy of preformed acrylic rubber dispersed clay filled epoxy nanocomposites, *Polymer* **46**, 11255--11262, 2005.
18. Kumar, P., et al. A review of experimental and modeling techniques to determine properties of biopolymer-based nanocomposites, *J. Food Sci*. **76**, E2--E14, 2011.
19. Ahmed, S. & Jones, S. R. A review of particulate reinforcement theories for polymer composites, *J. Mater. Sci.* **25**, 4933--4942, 1990.
20. Rafiee, M. A., et al. Enhanced mechanical properties of nanocomposites at low graphene content, *ACS Nano* **3**, 3884--3890, 2009.

21. Thakur, S. & Karak, N. Bio-based tough hyperbranched polyurethane-graphene oxide nanocomposites as advanced shape memory materials, *RSC Adv*. **3**, 9476--9482, 2013.
22. Ramakrishna, S., et al. Modified Halpin-Tsai equation for clay-reinforced polymer nanofiber, *Mech. Adv. Mater. Struc.* **13**, 77--81, 2006.
23. Phua, S. L., et al. Reinforcement of polyether polyurethane with dopamine-modified clay: the role of interfacial hydrogen bonding, *ACS Appl. Mater. Interfaces* **4**, 4571--4578, 2012.
24. Pongprayoon, T., et al. Antimicrobial resistance of clay polymer nanocomposites, *Appl. Clay Sci*. **86**, 179--184, 2013.
25. Barua, S., et al. Infection resistant hyperbranched epoxy nanocomposite as a scaffold for skin tissue regeneration, *Polym. Int*. **64**, 303--311, 2015.
26. Bagchi, B., et al. *In situ* synthesis and antibacterial activity of copper nanoparticle loaded natural montmorillonite clay based on contact inhibition and ion release, *Colloids Surf., B* **108**, 358--365, 2013.
27. Wu, Y., et al. Long-term and controlled release of chlorhexidine-copper(II) from organically modified montmorillonite (OMMT) nanocomposites, *Mater. Sci. Eng. C* **33**, 752--757, 2013.
28. Usman, M. S., et al. Synthesis, characterization, and antimicrobial properties of copper nanoparticles, *Int. J. Nanomedicine* **8**, 4467--4479, 2013.
29. Liang, X., et al. Preparation and antibacterial activities of polyaniline/$Cu_{0.05}Zn_{0.95}O$ nanocomposites, *Dalton Trans*. **41**, 2804--2811, 2012.
30. SaiRam, M., et al. Anti-microbial activity of a new vaginal contraceptive NIM-76 from neem oil (*Azadirachta Indica*), *J. Ethnopharmacol.* **71**, 377--382, 2000.
31. Ibrahima, N. A., et al. Antibacterial functionalization of reactive-cellulosic prints via inclusion of bioactive neem oil/βCD complex, *Carbohyd. Polym.* **86**, 1313--1319, 2011.
32. Ismadji, S., et al. Solubility of azadirachtin and several triterpenoid compounds extracted from neem seed kernel in supercritical $CO_2$, *Fluid Phase Equilibria* **336**, 9--15, 2012.
33. Anya, A. U., et al. Optimized reduction of free fatty acid content on neem seed oil, for biodiesel production, *J. Basic. Appl. Chem*. **2**, 21--28, 2012.
34. Das, G. & Karak, N. Vegetable oil-based flame retardant epoxy/clay nanocomposites, *Polym. Degrad. Stab*. **94**, 1948--1954, 2009.
35. Deka, H. and Karak, N. Influence of highly branched poly(amido amine) on the properties of hyperbranched polyurethane/clay nanocomposites, *Mater. Chem. Phys*. **124**, 120--128, 2010.

36. Konwar, U., et al. *Mesua ferrea* L. seed oil based highly thermostable and biodegradable polyester/clay nanocomposites, *Polym. Degrad. Stab*. **94**, 2221--2230, 2009.
37. Radhika, P., et al. Antibacterial screening of andrographis paniculata (Acanthaceae) root extracts, *Res. J. Biotechnol*. **3**, 62--63, 2008.
38. Roy, B., et al. Silver-embedded modified hyperbranched epoxy/clay nanocomposites as antibacterial materials, *Bioresour. Technol*. **127**, 175--180, 2013.
39. Djordjevic, D., et al. Microtiter plate assay for assessment of listeria monocytogenes biofilm formation, *Appl. Environ. Microbiol.* **68**, 2950--2958, 2002.
40. Wang, R., et al. Fabrication of bio-based epoxy-clay nanocomposites, *Green. Chem*. **16**, 1871--1882, 2014.
41. Maeda, Y. & Paul, D. R. Effect of antiplasticization on glass sorption and transport. III. Free volume interpretation, *J. Polym. Sci. Part B: Polym. Phys*. **25**, 1005--1016, 1987.
42. Pathan, S. & Ahmad, S. s-Triazine ring-modified waterborne alkyd: synthesis, characterization, antibacterial, and electrochemical corrosion studies, *ACS Sustainable Chem. Eng.* **1**, 1246--1257, 2013.
43. Pathan, S. & Ahmad, S. Synthesis, characterization and effect of s-triazine ring on physico-mechanical and electrochemical corrosion resistance performance of waterborne castor oil alkyd, *J. Mater. Chem. A* **1**, 14227--14238, 2013.
44. Wang, J., et al. Significant and concurrent enhancement of stiffness, strength, and toughness for paraffin wax through organoclay addition, *Adv. Mater*. **18**, 1585--1588, 2006.
45. Khan, S. B., et al. A thermally and mechanically stable eco-friendly nanocomposite for chemical sensor applications, *New J. Chem*. **36**, 2368--2375, 2012.